The Atmospheric Circulation

Thorsten Peters and Michael Richter

Contents

Abstract

Within this chapter the Hadley Circulation, the Monsoon System, Easterly Waves, Tropical Cyclones and the Walker Circulation are discussed. While the Hadley Circulation and the Monsoon System explain different air flow systems in a mainly meridional sense, a secondary system of latitudinal wind flow is governed by the Walker circulation which is decisive for the formation of La Niña and El Niño events. Apart from the long-term seasonal and nonseasonal variations of the tropical atmosphere, the climate of the Tropics is also affected by more frequent tropical weather disturbances. One of them are large-scale planetary waves which produce greater amounts of rainfall in many maritime tropical regions. These disturbance lines sprawl in a meridional direction from east to west and are called easterly waves.

Keywords

Easterly waves • Hadley circulation • Monsoon system • Tradewind system • Tropical cyclones • Walker circulation

T. Peters (✉) • M. Richter
Institute of Geography, Friedrich-Alexander-University Erlangen-Nuremberg, Erlangen, Germany
e-mail: thorsten.peters@fau.de; tpeters@geographie.uni-erlangen.de; sairecabur@web.de

L. Pancel, M. Köhl (eds.), *Tropical Forestry Handbook*,
DOI 10.1007/978-3-642-54601-3_36

Tradewind System and Hadley Circulation

The trade winds (also called trades) are the predominant surface winds towards the Equator in the Tropics. They are strongly related to the tropical atmospheric circulation which was described first by the English lawyer and meteorologist George Hadley in 1735. The initial trigger of this circulation is the intensive warming over the equatorial area where the surplus of heat energy leads to the uplift of air masses and to strong condensation processes and rainfall production. Within the equatorial zone, the heated air masses rise up to the upper atmosphere and are transported to higher latitudes by the anti-trades, which partially descent at about 25–35° latitude (Fig. 1, Lauer 1993). However, the denomination "anti-trades" proves awkward since it indicates a similarity to the surface trade winds although the anti-trades are neither equal in strength nor in steadiness. Instead, meridional components are weak and zonal components are strong. This could be traced back to the influence of the Coriolis force which is growing larger with increasing distance to the Equator. Because of earth's rotation moving air is deflected veering to the right of the moving

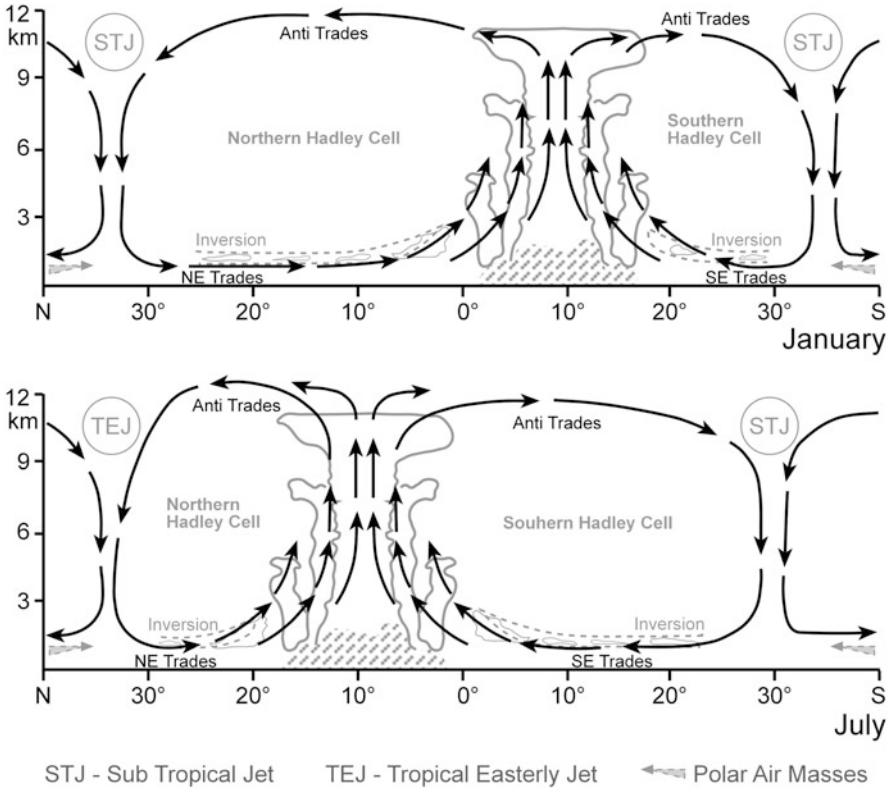

Fig. 1 Synoptic structure of the ITCZ (Inter Tropical Convergence Zone) (After Lauer 1993, Heyer 1998)

direction in the Northern Hemisphere and to the left in the Southern hemisphere. As a result, the upper air flows become more and more westerly at about 25–35° latitude and are named subtropical jets (STJ). Over the southern hemisphere the subtropical jet consists of strong winds at approx. 12,000 m altitude, which prevail throughout the year over 25–35° southern latitude. Over the northern hemisphere a similar jet stream is limited to the winter season. During the summer it is replaced by a strong easterly air flow over Asia and Africa, the Tropical Easterly Jet (Nieuwolt 1977; McGregor and Nieuwolt 1998). Between 25° and 35° latitude the cooling of air masses, the increased earth's angular momentum, and the accumulation of air masses due to the reduced size of the earth's surface lead to a broad subsidence of the air towards the ground. These areas are characterized by a relative high surface pressure and are called the subtropical highs. The Hadley circulation is closed by the quasi permanent trade winds from the subtropical highs towards the equatorial trough of low pressure. These surface winds are also deflected toward the west in both hemispheres by the Coriolis Effect and are known as the northeast trade winds in the Northern Hemisphere and the southeast trade winds in the Southern Hemisphere. The tradewind circulation consists of an internal cycle with an easterly current, which is forced by the structure of the subtropical high- pressure cells and an external cycle located between the extra tropical west wind belt and the tropical easterly current, where new air masses of polar origin are incorporated into the easterly current towards the Equator. Since air masses from both sides of the equator flow together at the Equator, the Inter Tropical Convergence Zone (ITCZ) is emerged. Its position is directly linked to the position of the thermal equator (zone of seasonal maximum temperature), and its migration towards the respective summer hemispheres occurs mainly in daily advances and retreats where diurnal changes of several hundreds of kilometers are possible (Lauer 1993). Both surface trade winds are limited to elevations about 500 m close to the subtropical highs and to elevations about 2,500 m close to the ITCZ and are also known as lower trades. The lower trades are very steady and mean wind speeds vary between 3.6 and 7.2 m/s with maximum wind speeds during winter. The air is usually humid and air temperature is affected by ocean's surface water temperatures, since the relatively cool air over the ocean water is heated from below and latent heat is absorbed. The lower trades are separated from the anti-trades by the trade wind inversion layer. The inversion layer is characterized by an increase in temperature with increasing altitude, and its thickness varies between 800 and 2,500 m close to the ITCZ. The tradewind inversion delimitates the lower layers of the atmosphere and inhibits the upward movement of humid air masses. Thus, rainfall does not occur, except where the inversion is lifted and largely destroyed. This is the case over the Equator and close to the ITCZ where the trades change direction or wind speeds are reduced. Within this area cumulus towers may occur at altitudes of 8–12 km which are accompanied by heavy rainfall and thunderstorms (Fig. 2). The trade winds will bring rain also in those cases, if an upward movement is caused by the relief. Heavy rains of that type fall on the east coasts of many tropical countries (e.g., Philippines, Madagascar, on the eastern slopes of the Caribbean and Central America, Hawaii, Surinam, southeastern Brazil, Vietnam, India, Northeastern Australia, and on the eastern escarpment of the Andes in South America). Over the

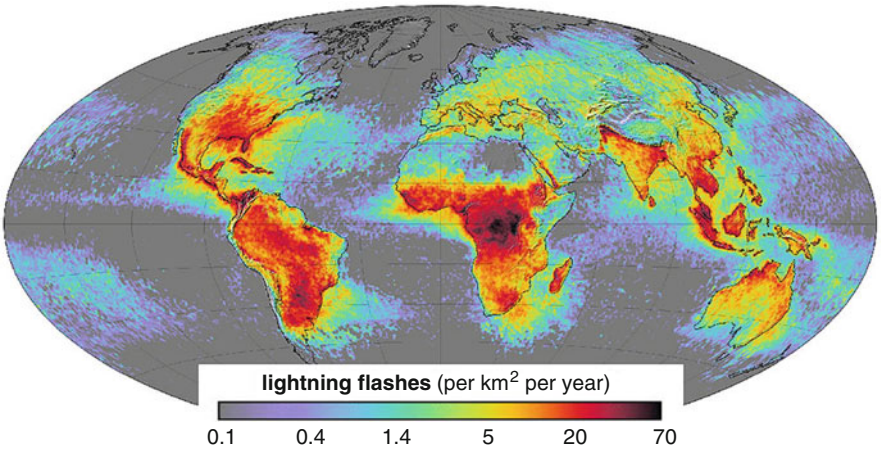

Fig. 2 World lightning map (Source: http://geology.com/articles/lightning-map.shtml, last assessed 5 May 2014)

Oceans, however, in the area of convergence of the trade winds, calms often occur which are called Doldrums or Mallungen (Lauer 1993; Nieuwolt 1977; McGregor and Nieuwolt 1998).

The northern as well as the southern Hadley Cell show strong seasonal variations in their intensity, regional extent and geographical position. Over the Atlantic and Eastern Pacific Ocean, the position of the ITCZ is clear cut in January and July and seasonal shifts are limited to 10° latitude on both hemispheres. Over the tropical continents the seasonal movement of the ITCZ is generally greater. This could be ascribed to the different distribution of landmasses and the different heat balance between land and ocean. Across the African Continent the ITCZ shows a similar oscillation pattern on both sides of the Equator which follows the position of the thermal equator and maximal surface heating. For the South American Area the ITCZ is strongly deflected towards the south during January and towards the north during July. Across the Indian and Western Pacific the oscillation patterns are clearly different from January to July. Here, the summer monsoons play an important role in explaining the seasonal behavior of the ITCZ and cloudiness (Fig. 3). In general, the oscillations into the Southern Hemisphere are smaller than those into the Northern Hemisphere, because the steady westerly circulation of the Southern Hemispheres middle latitudes constrains the equatorial through to near the equator (Lauer 1993; Nieuwolt 1977; McGregor and Nieuwolt 1998).

Monsoon System

The term “monsoon” originates from the Arabic Sea region where the Arabic word mausim means “season”. Traditionally, it was used for climate systems which show a clear seasonal large-scale shift of prevailing winds between winter and summer

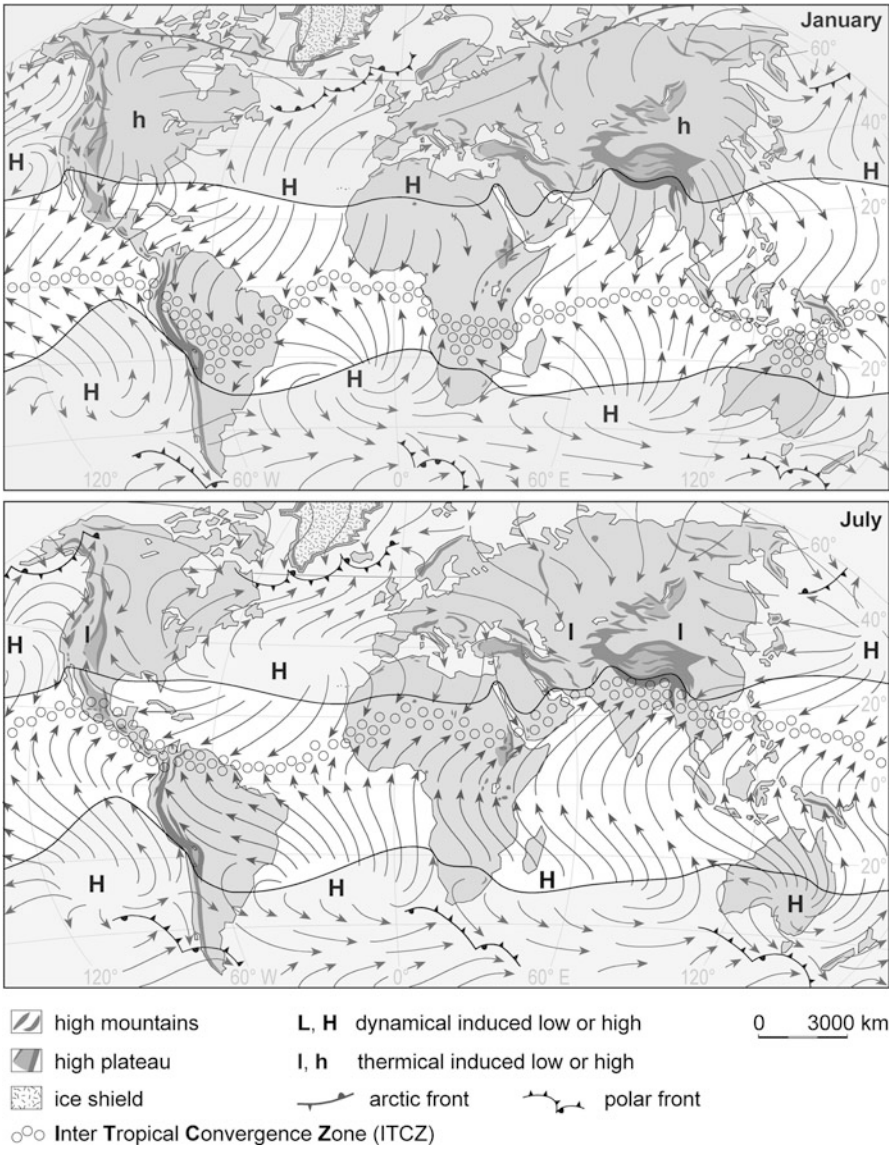

Fig. 3 Position of the ITCZ and predominant surface winds in January and July (After Richter 2001)

season. However, seasonal shifts of the surface winds occur in many regions that are not commonly considered as monsoonal and a combination of criteria is required for an adequate definition of monsoon areas (Barry and Chorley 2003). According to Ramage (1987) and McGregor and Nieuwolt (1998) the main characteristics of the monsoon regions are:

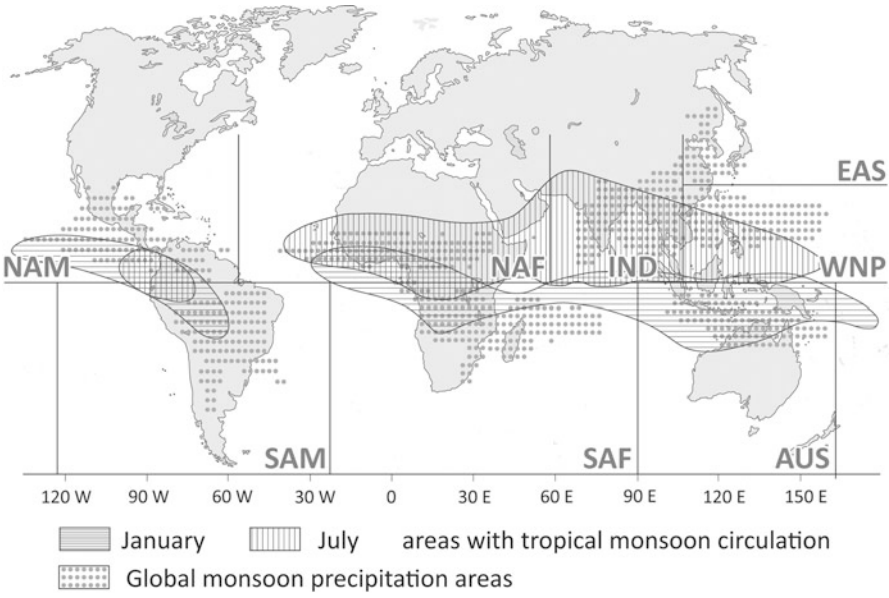

Fig. 4 Monsoon circulation areas (After Lauer 1993) and areas of monsoon precipitation (After WCRP 2013)

(i) The prevailing wind direction shifts by at least 120° between January and July.
(ii) The average frequency of prevailing wind directions in January and July exceeds 40 %.
(iii) The mean resultant wind in at least one of the months exceeds 3 m/s.
(iv) Less than one cyclone–anticyclone alteration occurs on overage every 2 years in any 1 month in a 5° latitude–longitude rectangle.

Following these criteria, the monsoon regions are distributed globally over all tropical continents and oceans (Lauer 1993). Although precipitation patterns are not included specifically, the seasonality in monsoonal rainfall is also an important attribute of the monsoon circulation (Dash 2005) (Fig. 4). Today, the best known regional monsoons are the North American monsoon (NAM), South American monsoon (SAM), North African monsoon (NAF), Indian monsoon (IND), East Asian monsoon (EAS), Western North Pacific monsoon (WNP), South African monsoon (SAF), and the Australian monsoon (AUS) (WCRP 2013). The fundamental drivers of the monsoon systems are the differential heating of land and ocean, the moisture processes in the atmosphere and the Coriolis Effect (Webster 1987). While seasonal changes in the tropical circulation are limited to minor latitudinal shifts and small variations in intensity over the large oceans, the situation is different over the tropical continents and nearby seas. Here, seasonal differences in land and sea surface temperatures lead to atmospheric pressure changes which cause the reversal of the seasonal prevailing wind systems. As moist warm air

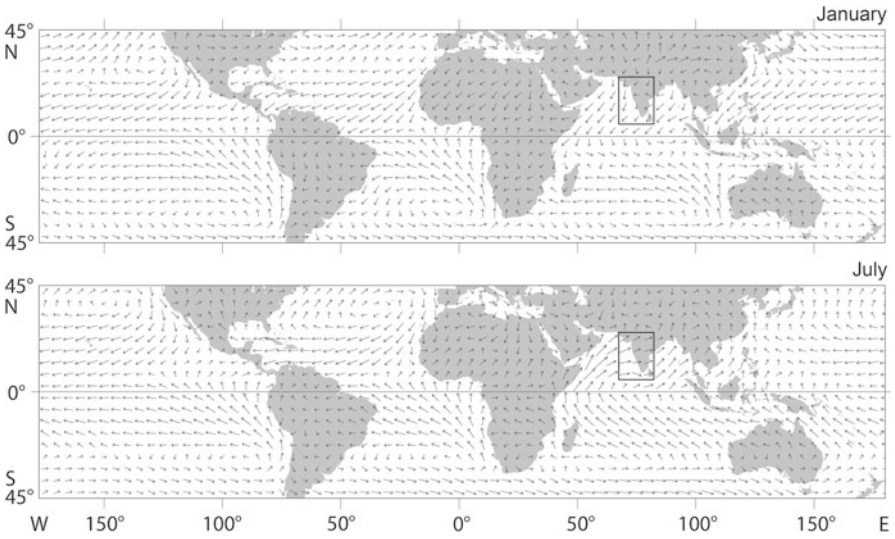

Fig. 5 Long term mean surface winds in January and July. Based on NCEP/NCAR Reanalysis dataset (2014)

masses rise over heated land masses, latent heat energy is released during condensation processes. This energy intensifies the pressure differences between land and sea regions and the intensity of the monsoon system. Furthermore, the Coriolis Effect deflects the northeastern and southeastern trade winds when they cross the Equator (McGregor and Nieuwolt 1998). Figure 5 shows the global surface circulation patterns during northern winter and summer and the land-sea circulation systems that generate the annual cycle of the monsoons. During January, the ITCZ is widely located southward of the equator and the regions of highest precipitation amounts are located in the southern hemisphere. In pre-summer, (April), the northern hemisphere tropical–subtropical land areas have started up warming but the thermal uplift of air masses is still weak. The northern hemispheres Hadley cell circulation as well as the offshore flow of air masses prevail and precipitation amounts are highest close to the equator and the ITCZ where moist air is raised into the troposphere by thermal convection (Fig. 5 upper panel, Fig. 6). As the thermal equator moves northward from May to June, the northern tropical landmasses are heated more intensely and the upward movement of air masses is getting stronger. This is leading to land-sea temperature differences, with the land being warmer than the surrounding oceans, which trigger a low-level flow of moist air masses from nearby oceans. Thus, the predominant wind directions change and the surface winds turn onshore (Fig. 5 lower panel, Fig. 6). Between June and July the heating of land masses, the uplift of air masses and the atmospheric moisture content are maximal and the monsoon reaches its maximum intensity. Latent heat energy released by convection, high above the land surface helps to pull in additional moisture maintaining the wet season. At this stage, the amount of precipitation and its

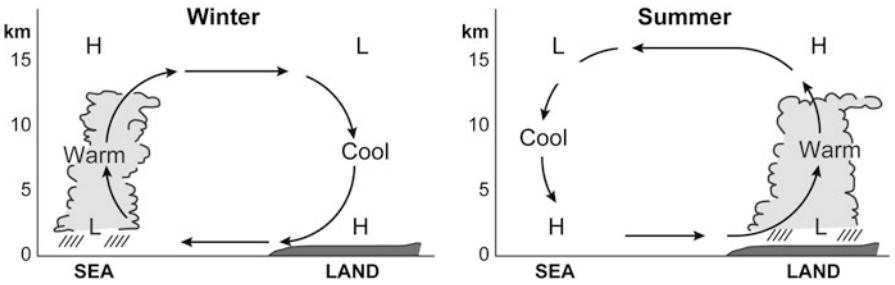

Fig. 6 Vertical circulation patterns over monsoonal regions (e.g., *black rectangle* in Fig. 5) during winter and summer (After Ramage 1987)

northward dimensions have reached a maximum too. As the thermal equator starts moving southward during September, the surface heating weakens and the structure of the monsoon is getting similar to the monsoon structure in April (Webster 1987; McGregor and Nieuwolt 1998; WCRP 2013). Thus, in general the summer monsoons of both the hemispheres are very wet and winter monsoons are dry and the monsoon system is directly linked to the position of the thermal equator and its annual migration (Dash 2005). Comparisons of seasonal wind directions in Fig. 5 show that the monsoonal circulation changes are best developed on a large scale in east and south Asia, with winds from southwest in summer and from the northeast in winter. The Asian summer monsoon consists of the Indian monsoon and the East Asian monsoon which are separated by the Himalayan mountain range. The Indian Monsoon is composed of the monsoon trough, the Mascarene high, the Tibetan anticyclone, the low level cross-equatorial jet, the upper level tropical easterly jet, Monsoon disturbances, and monsoon cloudiness with high rainfall amounts (McGregor and Nieuwolt 1998; Dash 2005). During north-hemispheric summer (JJA) the monsoon trough is located over northern India as part of the global ITCZ. Within its dynamic structure, south-westerly winds predominate at the south and north-easterly winds at the north. At the same time the Mascarene high is situated over the southeast Indian Ocean within the southern hemisphere. From this region, the air moves northward over the equator and turns to the east under the influence of the Coriolis force. These winds are known as the cross-equatorial East African of Somali jet and flow over the southern Arabian Sea and arrive over the central west and southern coast of India. During June – August these air flows are most intensive and split into two flow lines at around 10°N, 60°E. At the same time the heating of the Tibetan plateau is leading to the development of an upper level anticyclone with strong east north easterly air flows over north India. Within this zone, deep convection exists along with strong vertical wind shear. After September the Indian anticyclone moves in a south-southeastward direction as the thermal equator moves to the south. With this development the upper atmosphere easterlies associated with the easterly jet are replaced by the westerly's (McGregor and Nieuwolt 1998; Dash 2005). The East Asian summer monsoon can be divided into the cold anticyclone in Australia, the cross-equatorial jet at about 110°E, the monsoon

through and its zones of convection in the South China Sea and western Pacific, the upper level tropical easterly jet, the western Pacific high, the subtropical convergence (which is also called Mei-Yu frontal zone in China or Baiu frontal zone in Japan) and the mid-latitude disturbances (McGregor and Nieuwolt 1998; Dash 2005). During northern summer, East Asia's weather is determined by a large, thermally induced low-pressure cell that extends from the Arabian Peninsula to central China and from central India to Central Asia (Dando 2005). The monsoon trough extends from the western Pacific across Indo-China and is distinguished by wet, cloudy and often windy weather. For most of the time it is separated from the monsoonal trough over the Bay of Bengal and India associated with the Indian monsoon. In addition to the cross-equatorial flow from the southern hemisphere, the East Asian monsoon also originates from the Indian summer monsoonal airflow from the Indian Ocean and the southeast monsoon airflow from the western flanks of the Pacific high. The cross-equatorial flow is intensified when the pressure gradient between the Australian high and the thermal low over China is increased. Over the Malaysian Peninsula the cross-equatorial flow meets the westerly Indian monsoonal flows and large amounts of rainfall are produced in this zone of confluence. At the same time, a subtropical high is located over the western Pacific region and the southeast Asian summer monsoon forms. During July – August the western Pacific high moves quickly northward, as does the ITCZ to the south west. When the subtropical high moves westward over warm ocean surfaces it is rapidly modified and becomes unstable as it turns northwestward. At this moment, moist warm air from the southeast arises over the Philippines and into northeastern, southeastern and southern parts of Indo-China, China, and Japan. In general, the southeastern part of the East Asian monsoon is best developed over the South China Sea and southern China and Japan. Thus, the summer monsoon is often referred to southeast monsoon in these areas (McGregor and Nieuwolt 1998; Dash 2005).

Easterly Waves

Apart from the long-term seasonal and nonseasonal variations of the tropical atmosphere, the climate of the Tropics is also affected by more frequent tropical weather disturbances. One of them are large-scale planetary waves (with a wavelength of approximately 15° longitude) which produce greater amounts of rainfall in many maritime tropical regions as for example, in the Atlantic-Caribbean area and the South Pacific, but also over land, as for example, at the southern rim of the Sahel Zone in Africa. This disturbance lines sprawl in a meridional direction and are accompanied by irregular thunderstorms close to the ITCZ. As they move from east to west, they are called easterly waves. In the Atlantic Ocean, easterly waves generally arise at about 15°N, move westward at approximately 8 m/s and have a wavelength of 2.000–4.000 m. Their average lifetime is around 1–2 weeks (Fig. 7). Although they differ in size and intensity, they have one feature in common. Their main center of low pressure is not circular or elliptic, but in the form of a wave in the isobaric pattern. The genesis, maintenance, and development of easterly waves

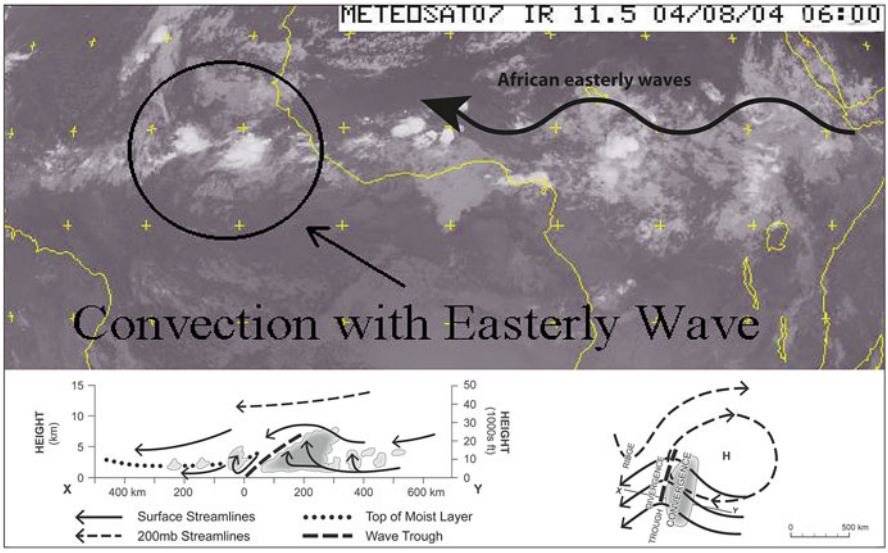

Fig. 7 Upper sketch: An African easterly wave (Source: http://www.fcst-office.com, last assessed 5 May 2014). Lower sketches: A model of the vertical (*lower left sketch*) and areal (*lower right sketch*) structure of an easterly wave. Cloud is stippled and the precipitation area is shown in the *vertical* section. The streamline symbols refer to the areal structure and the *arrows* on the *vertical* section indicate the *horizontal* and *vertical* motions (After Barry and Chorley 2003)

are linked to a complicated inter-relation between adiabatic dynamics, boundary layer, moist, and radiative processes. For their maintenance barotropic processes (within a barotropic atmosphere the density depends on the pressure, isobaric surfaces are parallel to isopycnic surfaces) are more important over the oceans while baroclinic (within a baroclinic atmosphere the density depends on the pressure and the temperature, isobaric surfaces intersect isopycnic surfaces) processes are more important over land. Easterly waves are commonest over the western Atlantic while their maximum amplitude could be located over the West African region. Here, they arise in a baroclinic–barotropic instability of the African tropospheric easterly jet. A typical easterly wave covers a large area and is usually relatively weak near the surface. Its averages low-level speed is slower than the basic current whereas the wind speeds in the upper levels may be equal to the speed of the basic trade wind current. The waves are strongest developed at the 700 mb level where vorticity is at a maximum. Ahead of the easterly wave, the east or northeast trade wind backs to northeast or north and air flow is divergent. Behind the wave, however, air is strongly convergent. Low-level divergence and high-level convergence are accompanied by subsidence and suppressed convection. As air behind the trough axis has a northward component it gains both absolute and relative vorticity as it approaches the trough axis. Consequently there is a vertical stretching of the atmospheric column which encourages low-level convergence. The opposite is true ahead of the wave as air here has an equator ward flow so the

vorticity components decrease. Consequently, there is vertical shrinkage of the atmospheric column and thus horizontal divergence. These contrasting patterns of divergence and convergence, westward and eastward of the trough axis respectively, produce contrasting weather patterns such that ahead of the easterly wave the weather is particularly fair as the trade wind inversion is temporarily reinforced and moved to a lower level by the subsident air. At the rear of the main axis, in the zone of convergence, squall lines prevail and the trade wind inversion is destroyed. Easterly waves are climatologically important as they bring large amounts of rainfall to areas which are generally dry as long as the trades are undisturbed. Fully developed or remnant easterly waves often provide the initial disturbance required for the development of tropical cyclones (Barry and Chorley 2003; Lauer 1993; McGregor and Nieuwolt 1998; Oliver 1987).

Tropical Cyclones

Tropical cyclones are normally restricted to areas of tropical oceans and coasts, but may also enter maritime Northeastern America and Eastern Asia. They originate from basins containing large bodies of warm water of at least 26.5 °C down to a depth of 60 m. When such a situation persists over days, the overlying atmosphere may become unstable and produces strong, (so-called) organized convection and thunderstorms. The strength of a resultant low pressure cell depends on its low-level vorticity, stability, and size, which is inversely proportional to the latitude and thus can reach very large dimensions in the tropics beyond 5°N and 5°S. For the forward motion of tropical cyclones atmospheric disturbances are needed to give an impetus, which in the North Atlantic and North Pacific Ocean is provided by African easterly waves. The latter are perturbations with periods of roughly 3–5 days and spatial scale of about 1,000 km. They emerge within the tropical easterlies, which act as a steering flow for tropical storms causing winds to converge and encourage the formation of cloud towers on the east side of the wave (Fig. 7). Although most parts of the inner tropical oceans exceed the required temperature, the cyclogenesis, through lack of exogenic spin forces (coriolis forces), never occurs within 5° of the equator and cyclones never cross this zone (Fig. 8, upper sketch). Instead, the tracks of most storms run westward- or westnorth westward and then often turn poleward when approaching the Tropics of Capricorn or Cancer. Hence, tropical cyclones arise from an initial disturbance over several steps into a tropical depression and eventually into a tropical storm stage. In a mature stadium, a hurricane or typhoon can envelop a diameter of more than 1,000 km, in satellite images eventually indicated by an all- embracing and overlapping thick cloud shield of a cumulonimbus anvil (Fig. 8, lower left sketch). During its evolution, latent heat, the main energy source of a tropical storm, is transferred from small cumulus clouds into spiral cloud bands and finally discharge into a complex of circularly arranged cloud towers (Fig. 8, lower sketches). Below the resulting cloud corpus, convergent air flows enter the ring of clouds and the central convection cell, which then develops from the interaction of various cumulonimbi. Here, a strong upward vortex picks up

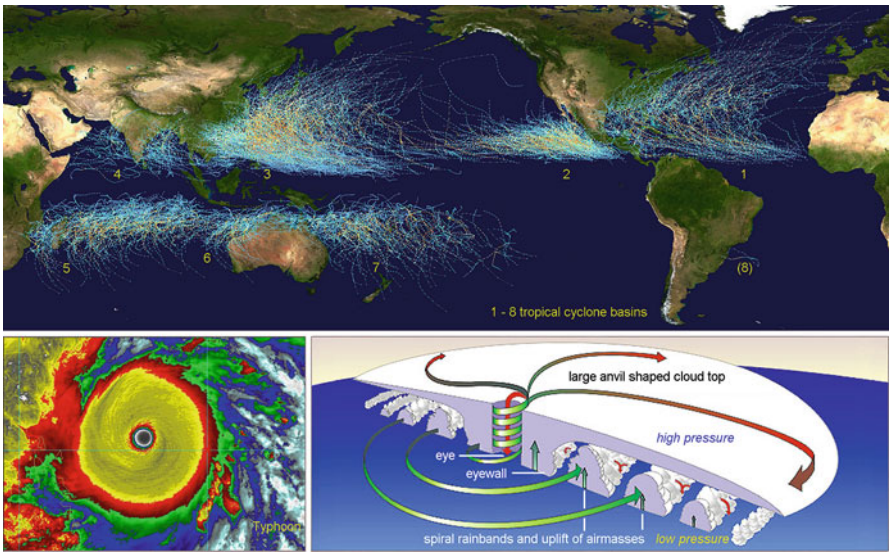

Fig. 8 *Upper sketch*: Tracks of all Tropical Cyclones which formed worldwide from 1985–2005. The points show the locations of the storms at 6-hourly intervals and use the color scheme of the Saffir-Simpson Hurricane Scale (Source: http://en.wikipedia.org/wiki/File:Global_tropical_cyclone_tracks-edit2.jpg, last assessed 3 May 2014). *Lower left sketch*: Super typhoon Haiyan during landfall on the central Philippines in 11 November 2013; colors indicate the surface temperature of clouds with *yellow* as coldest (*high central tower*) to *blue* as warmest part (sea surface) (Source: http://www.washingtonpost.com/blogs/capital-weather-gang/files/2013/11/1461780_624520054271903_1498249114_n.jpg, last assessed 24 Apr 2014). *Lower right sketch*: Cross section through a typical cyclone formation of an expanded cloud top (Modified from http://www.atmos.washington.edu/%7Ehakim/301/hurr_cross.jpg, last assessed 19 Feb 2014)

the warm and humid air tangentially into the base of the circular cloud wall around the central eye of the cyclone. In contrast to the violent uplift within its eye wall, downward air flows release an adiabatic warming by latent heat through condensation into the central eye (see isotherms in Fig. 9). In case of hurricane Gilbert, which crossed the Caribbean and the adjacent Gulf in September 1988, the air temperature reached surprising 28 °C at an altitude of around 3,100 m a.s.l. (Fig. 10). The high-level outflow causes an extremely low pressure within, and high maximum wind speeds around the storm center. The warm core promotes the hurricane as it intensifies the superimposed anticyclone at the upper tropospheric level and stimulates the low-level influx of warm and moist air. Thus, the described feedback system continuously boosts the convective activity and latent heat of a storm as long as it crosses a warm tropical ocean. In case of hurricane Gilbert, the storm grew in intensity between Jamaica and the coast of Yucatan, while after landfall, the high friction over land and the lack of latent heat intake impeded the storm's self-sustaining dynamics and it was rated down to a lower storm category (see SSHS in Table 1 and Fig. 10 upper sketch). The same hurricane is quoted one of the severest cyclones ever, since maximum gust speeds ranged up

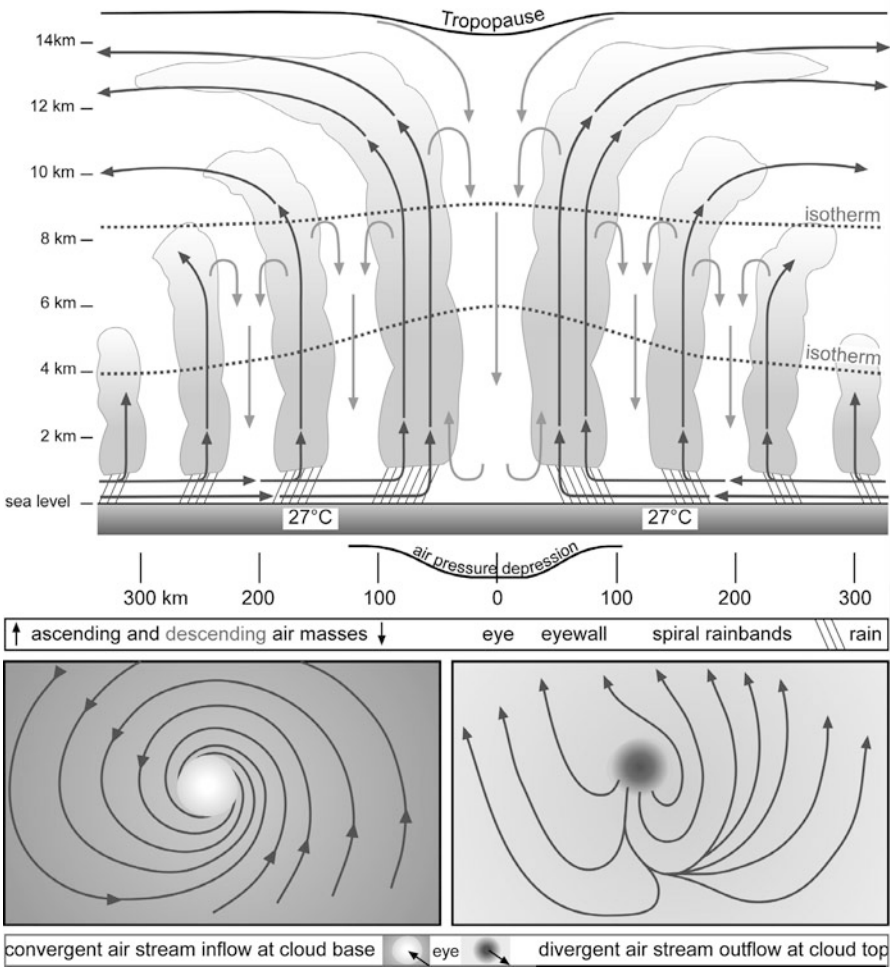

Fig. 9 Exemplary profile of a tropical cyclonic vortex (*above*) and sketches of convergent and divergent streams into and off the central eye (*below*) (composed by using information of various authors)

to 320 km/h and minimum air pressures down to 885 hPa. Such data are collected by "hurricane hunters", i.e., aircrews that fly into cyclones to monitor their formation on routine weather reconnaissance tracks by radiosonde transmissions (dropsonde system).

The maximum wind speeds of a hurricane or typhoon typically concentrate on the rotating air around the eye wall. The air in the eye itself stays virtually calm; the latter has a diameter of 30–50 km. Contrasting to the storm's absolute wind speeds, the whole complex moves usually forward at relatively slow 15–25 km/h. For this reason, a storm affected coastal area often suffers of destructive effects including persistent torrential rains for hours or even days. In most cases, tropical cyclones do

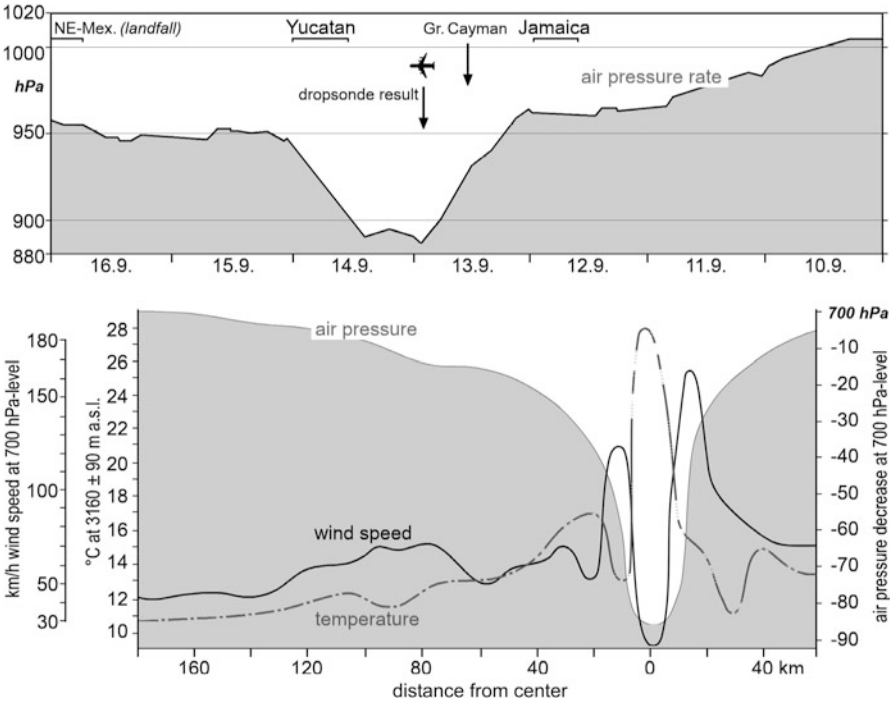

Fig. 10 Air pressure progression during the devolution of hurricane Gilbert over the Caribbean and the Mexican Gulf in September 1988 (*above*) and dropsonde results detected in the course of an aircraft crossing through the eye during strongest activity (*below*) (After Richter 1988)

Table 1 The Saffir–Simpson Scale (SSHS) for North Atlantic and Northeast Pacific hurricanes

Category	1	2	3	4	5
Wind speed (mph)	(74–95)	(96–110)	(111–130)	(131–155)	(>155)
km/h	119–152	120–177	178–209	210–249	>249
Central pressure (hPa)	>980	965–979	945–964	920–944	<920
Surge at coasts (m ↑)	1.2–1.8	1.9–2.7	2.8–3.9	4.0–5.5	>5.5

not make landfall but tend to veer off poleward in front of the eastern coasts of continents and travel along the western margins of subtropical high-pressure cells. However, this means that they may inflict an extended lane of damages alongside of these coasts as happens rather frequently at the island arc of the Northwest Pacific and the Bengal coast of the North Indian Ocean.

Worldwide, the Northwest Pacific exhibits by far the highest cyclone activity (Table 2), which threatens the coasts of Southeast Asia year-round. The background of the strong typhoon risk exposure of the western Pacific is attributed to its largest heat energy budget of the globe. In its tropical section it receives more energy than it gives off back into space, and thus results in extensive sea warming. Typhoon

Table 2 Season length, mean frequency (1968–2003) and regional denomination in tropical cyclone basins (frequency acc. to Schultz et al. (2005))

Basin	Cyclone season length	Mean frequency		Denomination
		Storm	Cyclones	
North Atlantic	June 1–November 30	10.6	5.9	Hurricane
Northeast Pacific	May 15–November 30	16.3	9.0	Hurricane
Northwest Pacific	January 1–December 31	26.7	16.9	Typhoon
North Indian	January 1–December 31	5.4	2.2	Cyclone
Southwest Indian	July 1–June 30	13.3	6.7	Cyclone
Southeast Indian	November 1–April 30	7.3	3.6	Willy willy
Southwest Pacific	November 1–April 30	10.6	4.8	Cyclone

Haiyan, as one of the strongest tropical storms ever at the time of landfall, brought wind speeds up to 310 km/h (195 mph) when it struck the Philippines (Fig. 8 lower left sketch). Fewer incidents are registered for the Northeast Pacific with little impact on ecosystems due to the lack of extended land masses. Here, storm systems turn into the open, westbound ocean. The once again fewer events in the North Atlantic are many times associated with most dramatic wind and gust speeds, ocean surges and rainfall amounts, but concentrate on early June to late November, with a sharp peak in late August through September. The surroundings of the Bay of Bengal suffer from very high vulnerability between May and November. Storms in the tropics of the southern hemisphere are generally weaker than those of the northern basins and peak in mid-February to early March.

North Atlantic and Caribbean hurricanes mostly start their life cycle close to the western African coast and are often called Cape Verde storms. They traverse a long trajectory over the warm ocean and consequently have a long time to develop and gain extreme intensity before reaching the Caribbean Sea or make landfall. Eastern Pacific tropical storms may even originate from them after crossing the narrow isthmus of Central America. In the basins of the western Pacific and northern Indian Ocean monsoon troughs are the main trigger for tropical cyclogenesis.

Tropical cyclones decay when entering landmasses as a result of the surface roughness or they undergo an extratropical transition when continuing their route as conventional low-pressure cells over cooler sea surfaces. Landfall impacts imply ecosystem disturbances or destructions by heavy wind gusts, creating gaps or clearings in forests. When hurricane Mitch struck the Honduras Bay Island "Guanaja" in October/November 1998 most trees of ample forests of native *Pinus caribaea* were uprooted, mangrove forests were almost completely ravaged, while gallery broadleaf forests survived without severe damage (Fig. 11 and Vanselow et al. 2007). Apparently, monospecific forests such as tropical pine stands suffer more from wind throw and uprooting than their multi-species counterparts, which in most cases are characterized by dense trunk and uneven canopy structures (see picture in Fig. 11 below). Research in South Florida forests of *Pinus elliottii* var. *densa* document that uprooting and standing dead are typical for tall trees which are most exposed to strong winds, while broken trees concentrate on lower levels of the

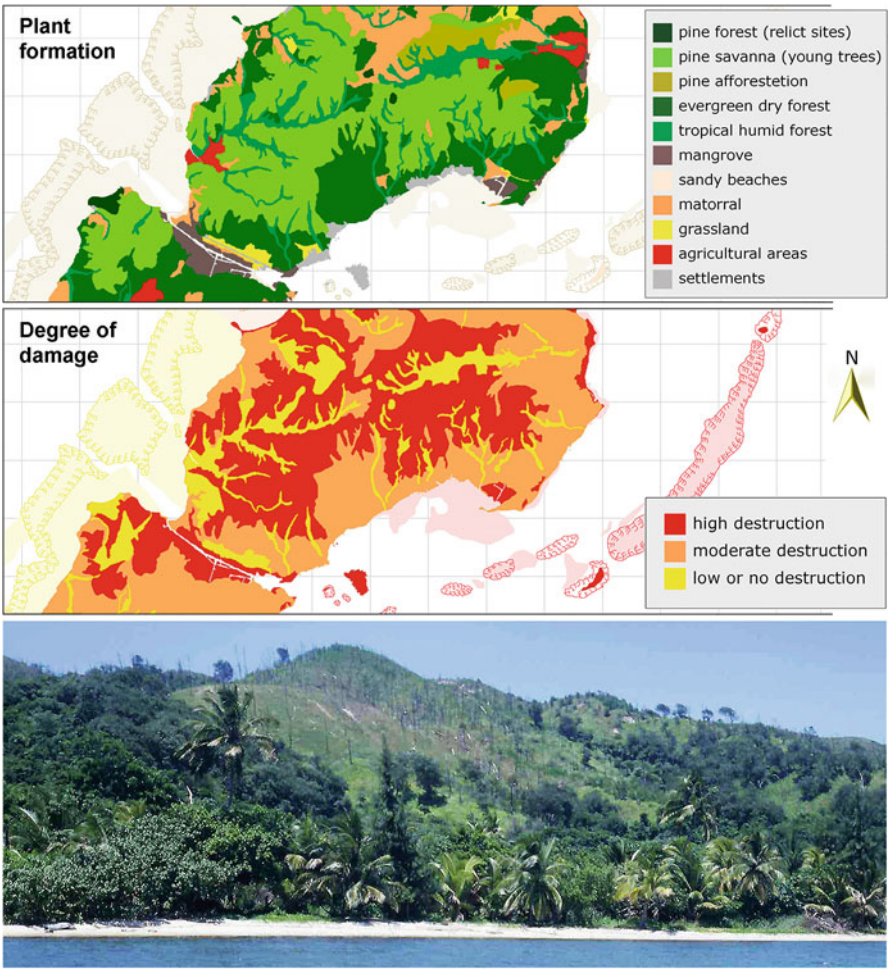

Fig. 11 Plant formations (*above*), destructions after Mitch 1998 (*center*; both extracted by maps of Vanselow et al. 2007) and picture taken in August 2002 of heavily destroyed pine (clearing) and scarcely affected broadleaf forests above the southeast coast of central Guanaja/Honduras (*below*)

population, partly damaged by collapsed branches of ambient overtopping trees (Fig. 12 above).

One more interesting result of the same investigation is the drop direction of uprooted trees. As a result of hurricane Andrew in August 1992, the contrasting position of uprooted trees as presented in Fig. 12 (below) shows a rather opposed fall direction between the two sites Pine Island and Lostman's Pine, which lie around 30 km away from each other. This opposite tendency of toppling over indicates the obvious phenomenon of a track of the hurricane's center right between both areas by first overthrowing the pines from southeast-directions and then after the passage of the calm eye from west.

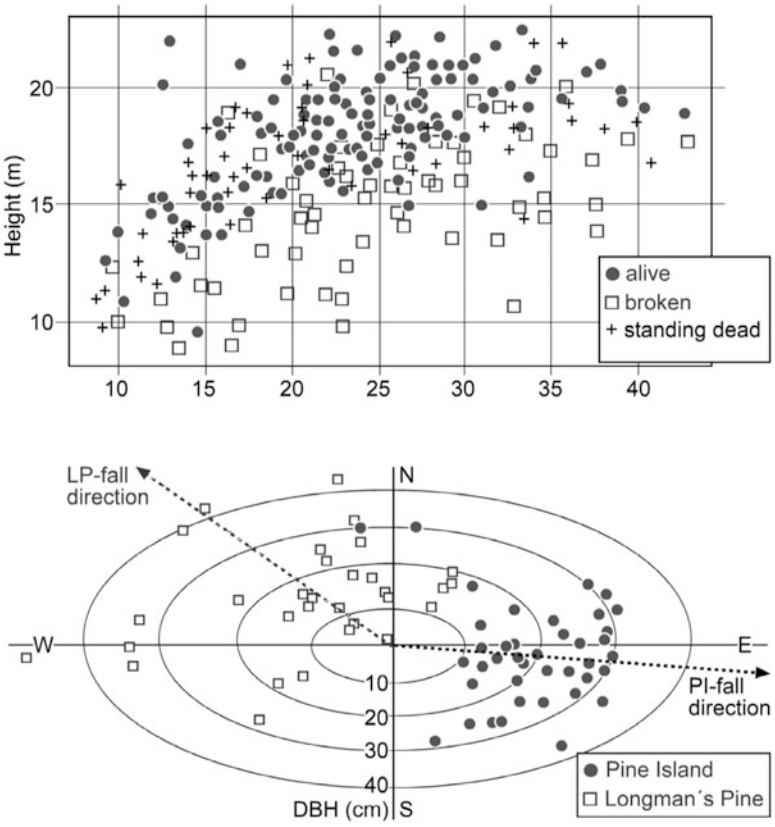

Fig. 12 Tree damage (*above*) and direction of uprooted pines (*below*) in southern Florida after the passage of hurricane Andrew in 1992 (acc. to Ross et al. 1997)

Interestingly, also phenological rhythm seems to be connected with cyclonic activity. Hamann (2004) underlines an obvious selective advantage for wind-dispersed species to fruit during the windiest time of the year, and all wind-dispersed trees do fruit during the typhoon season between July and November. Also, fruits solely dispersed by gravity are produced during this period since they might benefit from being more effectively dispersed during heavy storms.

While this type of impact is mostly restricted to coastal environments, heavy torrential downpours can also impair inland regions through landsliding, river erosion, and sedimentation. As hurricane Mitch had a very slow overall storm motion of less than 2 m s^{-1}, the resulting local enhancement of quasi-persistent rainfalls was extreme with reports of 911 mm for 7 days in October 25–31. However, the strength of a hurricane is not necessarily decisive for the degree of landscape damages. Faraway, hurricane Stan never exceeded class 1 according to the Saffir–Simpson scale (Table 1) but caused with disastrous rainfalls huge landslides and vast flooding, crushing ample areas of tropical mountain rainforest

alongside the Sierra Madre de Chiapas and the Volcanic Cordillera in Guatemala in September 2005 (chapter "▶ Microclimate in the Tropics", Fig. 8). Most of the Pacific escarpment of the two mountain chains was exposed to 2 days of excessive rainfall over 300 mm/day. For several weather stations in the drier part of the mountain, the statistical recurrence period for such an event is up to 500 years (Dekarski et al. 2012). Finally, short-time records of rainfall were observed during tropical cyclones, many of them for different weather stations on the island of Réunion. The highest precipitation value for 1 day ever measured was 1.825 mm in 7 January, 1966 at Foc-Foc during cyclone Denise. 10 day records of 5.677 mm were registered at 2.364 m a.s.l. from 18 January to 27 January, 1980 at Cratère Commerson during cyclone Hyacinthe. Here, as well as on several more tropical islands, lifts of deep tropical moisture over steep mountain escarpments result in large rainfall efficiency, like on various Philippine islands, where it rained 1.216 mm at Baguio in 15 October, 1967 during typhoon Carla.

The Walker Circulation and ENSO-Phenomena

While the Hadley cell explains a primary air flow system between the ITCZ and the subtropical high-pressure cells in a meridional sense, a secondary direction of latitudinal transport within the tropics is governed by the Walker circulation. The strength and location of these flows are decisive for the formation of La Niña and El Niño events. Worldwide attention was focused on El Nino 1997–1998 which affected various parts of the globe, when severe droughts and dramatic bushfires affected Indonesia and Brazil, while dramatic inundations and mosquito plagues involved the Sechura Desert in Peru.

Since then, nature scientists recognize that among the most prominent sources of asymmetric climatic variations on earth, the irregular El Niño Southern Oscillation (ENSO) cycle is of highest climate-ecological importance for many areas of the tropical zone. The El Niño phenomenon ("the boy" or "Christ Child" according to it's date of recurrence) is the most prominent event of the system and peaks at the end of each year of the southern hemispherical summer. At that time a weak, warm current flows southward and replaces the cold Humboldt Current along the coasts of southern Ecuador and northern Peru. Recently, apart from El Niño and its counterpart La Niña ("the girl") as two opposite phases of a planetarian scale oscillation, further circulations are detected, which must be seen as associated phenomena. One is the "Modoki", a kind of nontraditional El Niño, in which the usual positive sea surface temperature ENSO-anomaly near the coast of southern Ecuador and northern Peru does not occur, but stays in the central Pacific. One more type of interannual oscillation of sea surface temperatures (SST) is the Indian Ocean Dipole (IOD). During this anomaly the western part of the Indian Ocean becomes alternately warmer and then colder than the eastern part. Such events interact only to some extent with Pacific ENSO-system. All of the aforementioned phenomena are largely coupled with the Walker circulation system, a conceptual model of zonal and vertical air flows in the troposphere of the tropics depicted in Fig. 13.

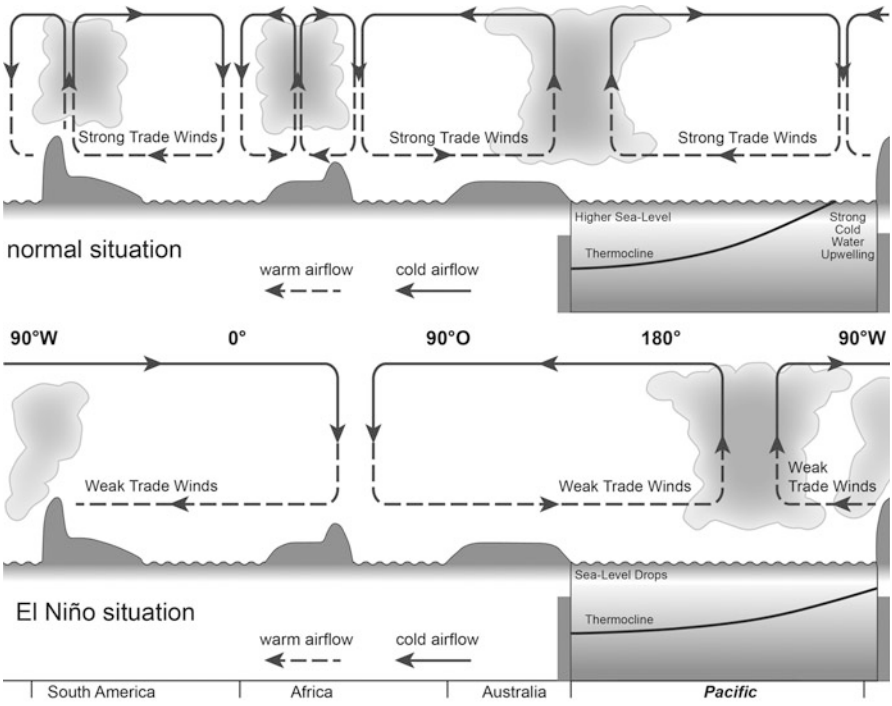

Fig. 13 The Walker circulation system of trade winds under normal and El Niño conditions and its impact on the sea level and the thermocline in the Pacific Ocean (composed by using information of various authors)

The Walker system or Walker cell is created by differences in the heat distribution between the tropical sections of the oceans and continents, where variations in rainfall, cloud cover, wind and temperature are generally governed by bimodal variations in pressure at sea level: the barometric "pressure seesaw" between Darwin (formerly Jakarta) and Tahiti, known as ENSO Teleconnection (see below). The air circulations of the tropical Pacific, Atlantic, and Indian basins result in easterly surface winds in the first and second basins and westerly winds during austral winter in the third one. Therefore, the three oceans display dramatic asymmetries in the sea surface temperature (SST) structure. The equatorial Pacific and Atlantic both have cool SSTs in austral winter (and spring) in the east, while cooler SSTs concentrate in the western part of the Indian Ocean. These thermic changes reflect changes in the depth of the thermocline, which is the transition layer between warm surface and cool deep water. Consequently, changes in strength, direction, and position of the Walker cell can influence cold water upwelling alongside the coasts of Chile, Peru, and Ecuador and thus, dictates the range of climatic variations within a major core region of ENSO-phenomena. In contrast to the upwelling of deep water in the east, the western half of the equatorial Pacific is characterized by trade winds from the east piling up warm superficial seawater.

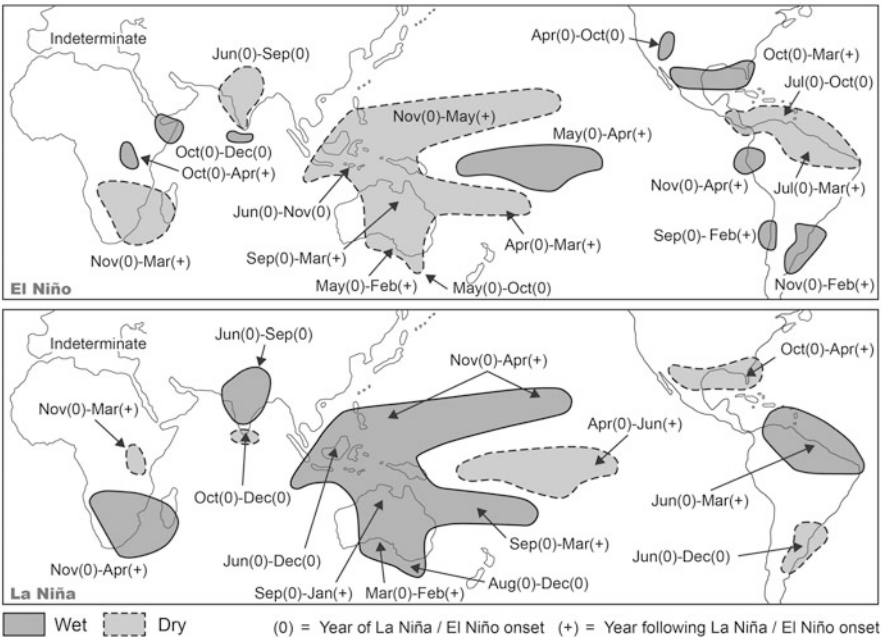

Fig. 14 Regions of increased precipitation and drier conditions during El Niño and La Niña phases (acc. to Allan et al. 1996)

Here, moist air and low pressure weather comes along with thunderstorms and typhoons. Due to the wind-driven westward motion of surface water, the ocean surface is some 60 cm higher in the western Pacific, from where downwelling initiates a compensating return flow of deep seawater to the east.

However, while the worldwide connection between ENSO events and precipitation, temperature variability, and appendant wind traits is increasingly well understood, little is known about the drivers of the system. Suggestions for the initial forcing of ENSO range from correlations of phases within subcycles of the 11.1-year sunspot cycle and their maxima usually occurring 2–3 years before the peak of an El Nino (e.g., Landscheidt 2000) over a still undefined weakening of the trade wind system to speculative impulses through the thermohaline circulation. Driven by differences in the temperature and salinity of seawater, the latter describes a highly complex conveyor belt which transports heat around the oceans on a scale of decades to centuries (Gnanadesikan et al. 2005).

Irrespective of these still open questions, the effects of ENSO particularly on precipitation and temperature can result in remarkable influences on plant communities of vast tropical ecosystems. Several areas are qualified as ENSO-core regions of which those affected by heavy rainfall during El Niño concentrate often around the Argentine–Brazil border, the Horn of Africa, on southernmost India, continental Southeast Asia, and especially on the west coast of tropical and central South America (Fig. 14). Here, rainfall inputs vary considerably with around double in north-central

Chile and up to more than 50 (!) times higher than normal in the Sechura Desert in northwestern Peru, which is identified as the world's most sensitive El Niño-ecozone (Richter and Ise 2005). In contrast, drought conditions may occur in north eastern Australia, Indonesia and the Philippines, islands of the central Pacific, northern South America, and the Caribbean, furthermore in southeastern Africa and northern India. These shifts of the rain and the dry zones are coupled with a weakening of the trade winds due to displacements and slackening of tropical pressure cells, above all of the low over the western and the high over the southeastern Pacific.

The pressure fluctuations between these two pressure cells are expressed by the Southern Oscillation Index (SOI, Fig. 15) with El Niño episodes associated with negative values, La Niña with positive values, meaning below normal pressure at Tahiti, and above normal pressure at Darwin (Australia). A further valuable measure is given by indices of SST anomalies such as the "Cold Tongue Index" (CTI). It describes a narrow latitudinal band extending from mainland Ecuador to Galapagos and beyond, expressing eastern equatorial Pacific sea surface temperature anomalies (Fig. 15). Furthermore, a "Multivariate ENSO Index" (MEI) is based on six variables observed over the tropical Pacific including measurements of specially equipped buoys. These and further indices allow limited forecasts on the arrival of ENSO phenomena. Having said that, uncertainties on the development of the foreseeable event persist especially for areas away from the eastern Pacific. Such is the case for the Dipole system along the western Indian Ocean, where the regions affected by wet and dry El Niño-impacts may vary considerably. Also, the location of areas in the western half of the Pacific pressure seesaw suffering from droughts during El Niño may differ notably over time and space between the vast sectors extending from insular East Asia to eastern Australia. The only region of stable repetitive occurrences of the phenomenon is the western coast of South America, at least in the event that Modoki as sort of a premature decay of the system's progress does not occur.

El Niño begins at the time when the atmospheric pressure rises in the Pacific's west and falls in the southeast and the trade winds weaken. This induces surface water to move eastward from the warm seawater pool around insular southeastern Asia and northeastern Australia towards the central Pacific (Fig. 13). In front of the western coast of South America, the conventional cold water upwelling becomes suppressed by the lowering of the thermocline (below right in the same figure). The cutoff of the upwelling goes along with westerly wind bursts undermining the trade winds generating long "Kelvin waves" towards east and warming up the SST in the eastern Pacific causing an eastward migration of abnormal convective cloudiness and rainfall. In contrast to reliable, at least slightly enhanced El Niño rainfalls in the Sechura Desert of northwestern Peru, further ENSO prone wet areas must not necessarily be affected, neither must a contrasting drought situation occur in the complementary dry areas of the western Pacific. As demonstrated in Fig. 15, both "Super-Niños" 1983 and 1998 resulted in extraordinary rainfalls during austral summer and autumn at Paita in northern litoral Peru, while incoming precipitation at Cairns (NE-Australia) was almost normal, around 80–90 % of the annual mean, and with this by far higher than the annual minimum. Further south, instead,

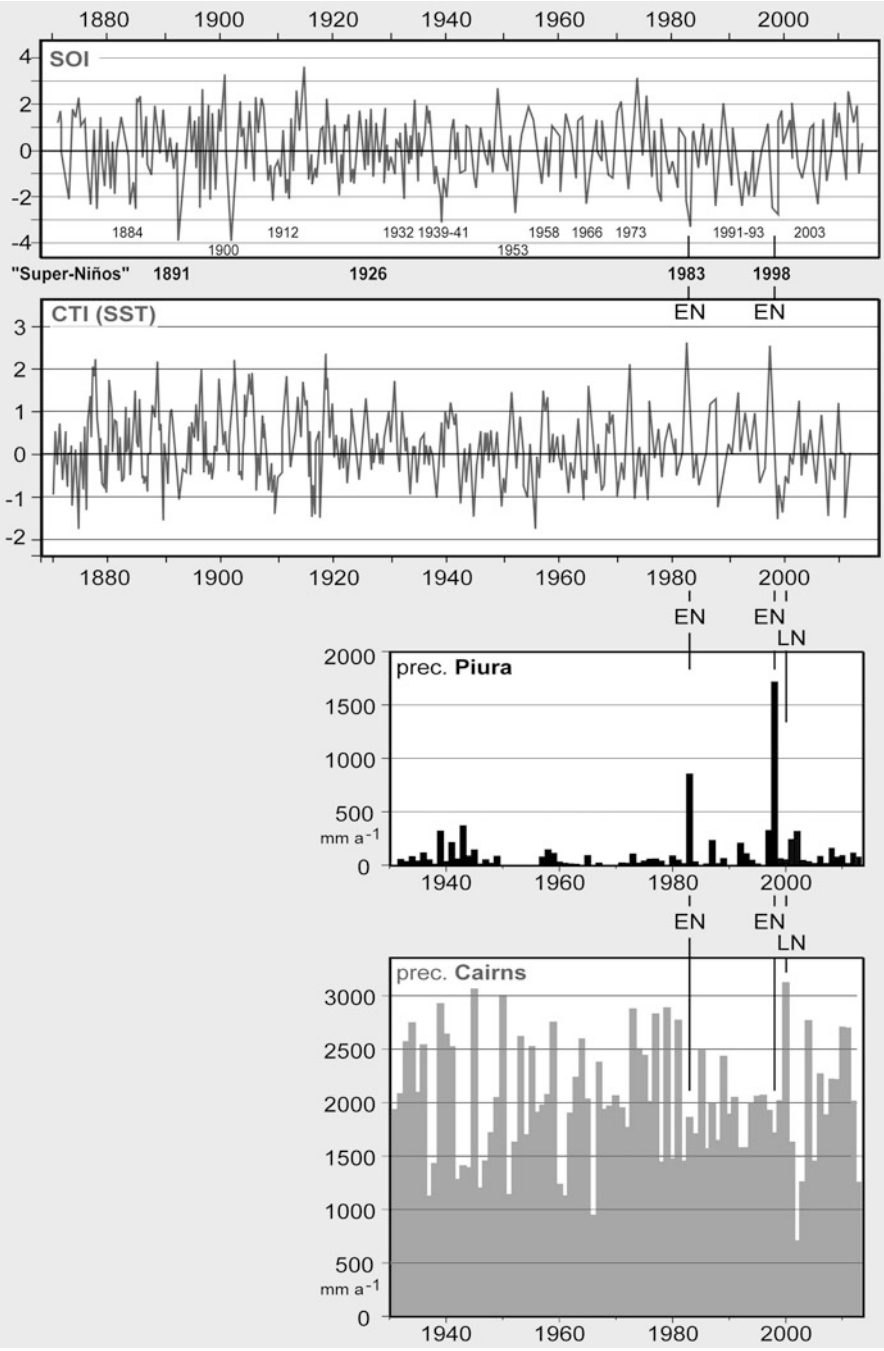

Fig. 15 (continued)

Mediterranean parts of Victoria experienced the driest 11 months on record up to the end of August 1997, hence in the run-up to the great event, while parts of Sumatra and even of Amazonia suffered from wildfires due to enduring desiccation.

Vice versa, an opposite effect can be seen in 1999, when a strong La Niña caused a record rainfall year at Cairns, whereas the annual amount at Paita was not less than average. Thus, a striking variability of the La Niña teleconnection seems to govern the western coast of South America (Fig. 14, below). The deserts of Atacama, Peru, and Sechura are not identified as strongly desiccated areas during La Niña because apart from El Niño-impacts they are anyway dry. The oscillation time between both ENSO counterparts of the Pacific basin is irregular, but generally occurs once every 2–6 years with El Niño-phenomena lasting normally between 6 (Modoki) and 18 months. Longer events can peak in "double Niños" as was the case in 1939–1941 and in 1991–1993 (Fig. 15). La Niña phenomena can last even up to 3 years, which happened in 1973–1976, and also immediately after Super-Niño 1998, cooler than average temperatures, SSTs prevailed long during 1999–2001 (Fig. 16). The overview of 17 consecutive years reflects that yellowish-reddish as well as dark blue SSTs form the same "tongue" drifting off from the Ecuadorian coast. Evidence for prominent La Niña excursions are visualized for April – December 2007 and July – December 2010, i.e., just the phase when El Niño rainfalls do not touch the area. However, while the coast at Paita stays dry during such events, Chulucanas 90 km inland can receive above average precipitation from moist air spilling over the Andes. Solar heating destabilizes the local troposphere during austral summer and easterly winds transport the moisture from Amazonia towards the Pacific coast.

Once again El Niño 1997/1998 and once again the Pacific coast of South America can serve as an example for surprising differences between the impact of one single ENSO phase. In contrast to the rain-loading conditions in northwestern Peru, the central and southern coasts of the country as well as of northern Chile, received below average precipitation during the same period (Fig. 17). Analyses by Bendix and Bendix (2006) suggest that high SSTs in combination with strong SST gradients along the "cold tongue" and warm SST bubbles in the vicinity lead to spatiotemporally varying patterns of different moist instability and rainfall inputs. Both, the reversal of the Walker cell on spot and an extended land-sea breeze system contribute to spatial divergences in El Niño rainfalls. Such factors might contribute to the fact, that for example Lima and Pisco experienced a below average rain rate during Super-Niño 97/98 while Tacna further south showed a slightly above normal rate. During El Niño years, this can be valid for further coastal desert parts in Chile too, at least concerning higher cloud-fog impacts. One more obvious

Fig. 15 Sea surface temperature anomalies (Cold Tongue Index = CTI, Southern Oscillation Index = SOI) and annual precipitation in Piura/northwestern Peru (El Niño and La Niña) as well as in Cairn/eastern Australia. (SOI acc. to http://math.ucr.edu/home/baez/soi-1876-1998.gif, CTI to http://www.jisao.washington.edu/data/cti/cti18502011.gif, Piura prec. acc. to data from SENAHMI, Lima Cairns prec. acc. to data derived from http://www.bom.gov.au/climate/data/)

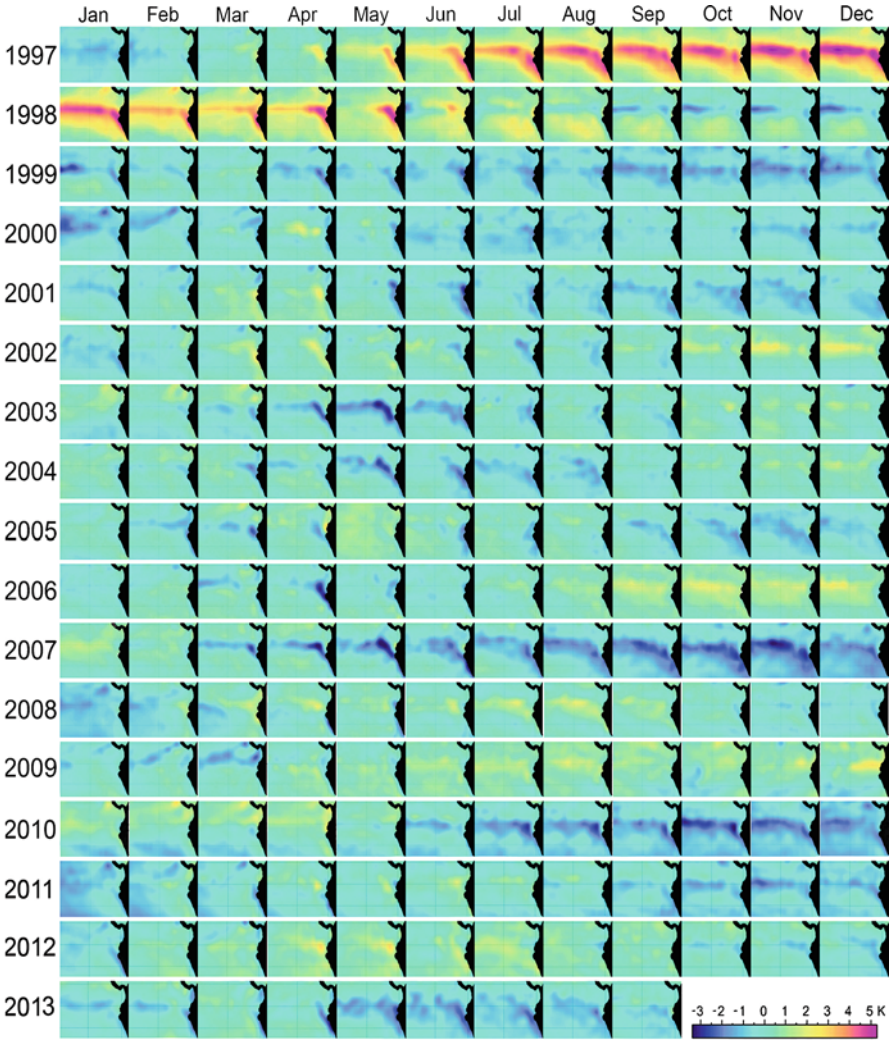

Fig. 16 Sea surface temperatures offshore west of northwestern South America ("Cold Tongue") between 1997, i.e., the start of "Super-Niño 97/98", and the end of 2013. *Yellowish* (up to *violet*) colors around October – February depict above average warm, *blue* below average cool SSTs or El Niño and La Niña phases, respectively (Data derived from the NCEP/NCAR dataset 2013)

rainfall gradient must be noted for the coastal hinterland and the adjacent Andean escarpment. Above the seaside towns of Talara and Lambayeque of above average values of 9.500 % and 6.700 % of rainfall respectively, the 1997/1998 event is reduced to values of 120–260 % between around Huarmaca and Cajamarca.

The decreasing relation of El Niño 1997/1998 to a normal year along the inland and altitudinal gradient becomes also visible by the comparison of the two precipitation maps in the upper part of Fig. 18. During this phenomenon, highest rain rates

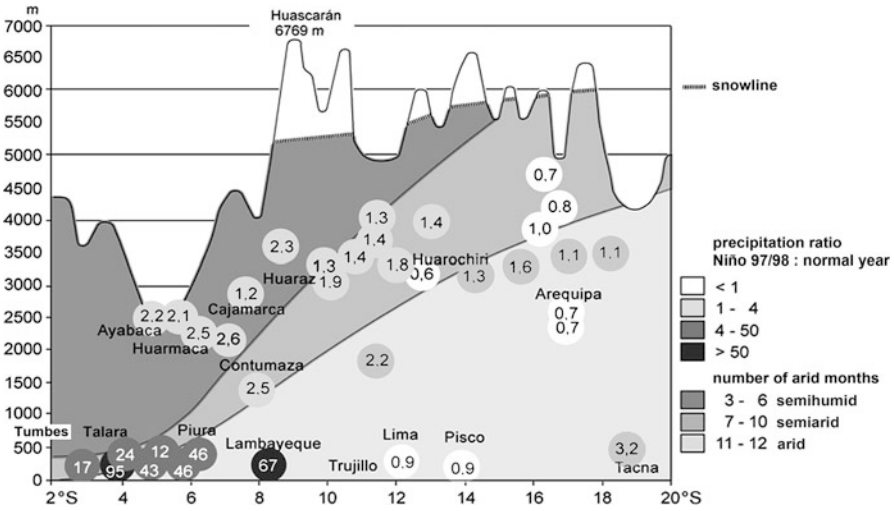

Fig. 17 Precipitation ratio between Niño 1997–1998 and a normal year at locations along the western escarpment of the Andes and the coast of Peru (acc. to data from SENAHMI, Lima)

were registered around Tambogrande and west of Macará, which still represent lowland locations in the foothills west of the Andean slopes. Further upwards and to the east, the rain amounts decrease during El Niño, while they decently increase during normal years (note: the crest line of the mountain chain is at right outside the two sketches shown). Chulucanas, one more center of torrential rains received a 12-fold amount in 1998, which in concrete terms meant 3,355 mm instead of only 201 mm under normal conditions. Also minor El Niño- or even Niño-like events caused by warm water vesicles in front of coastal Paita may result in most effective downpours at Chulucanas. In March 2002, a temporary phase of locally enhanced SST anomalies of +3 K generated maximum amounts of 75 and 115 mm d–1 of rainfall within 3 days.

Ecological consequences of such anomalous wet events on vegetation of tropical dry lands are dramatic and can also be long-lasting. In the Chulucanas area they were and still are characterized by the following steps of plant succession (Fig. 18):

- Pre-Niño stage with few half-shrubs and shrubs (*Encelia* and *Acacia*, *Cordia*, resp.), but no herbs.
- Initial boom of herbaceous, mostly annual grasses and herbs, for few months up to one and a half year during and after EN 97/98.
- In late September 1998, large surface fires due to the straw accumulation destroyed the herbaceous layer but did not affect shrubs and trees.
- Continuous upcoming growth of *Acacia* through the following 5 years accumulating to around a coverage of 80 % after 10 years due to consecutive EN (and LN) rainfalls in 2001, 2002, and 2008.
- Slight decrease of shrub cover after 2010.

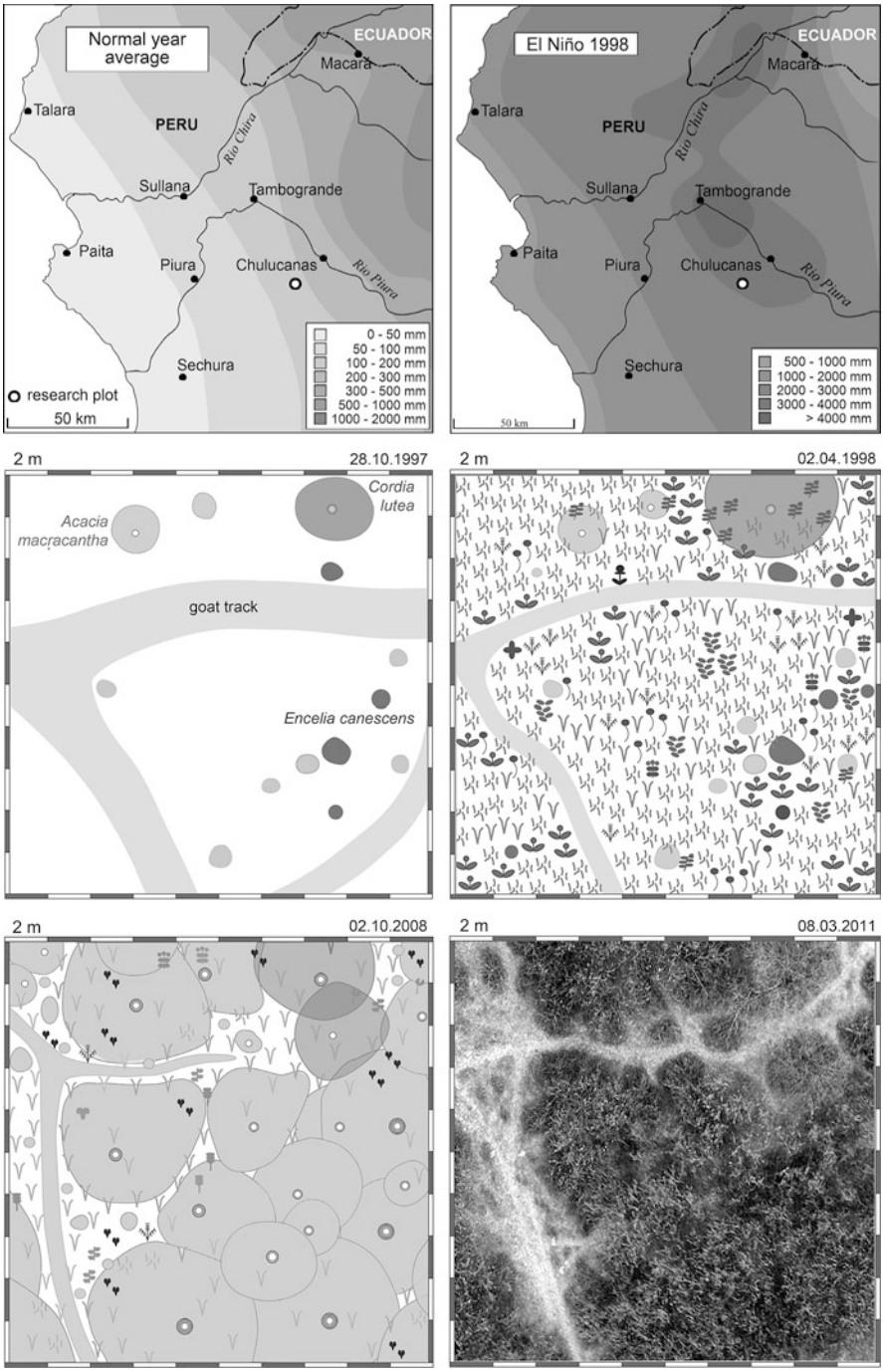

Fig. 18 (continued)

Trees of algarobbo (*Prosopis pallida*) and zapote (*Capparis scabrida*) are not established within the 400 m^2 plot of the sketch map, but are widespread in the ambience and profited from the rainfalls too. The depicted shrubification seems to reflect a positive trend, but after several "fat years" must be considered overgrazing effects and sort of degradation, since *Acacia macracantha* only serves as emergency nutrition for malnourished livestock, which additionally diminishes the carrying capacity by heavy trampling. Nevertheless, enhanced productivity from El Niño precipitation contrasts with widespread effects of desertification. Although being only a temporal event, a recovery during the post-Niño phase may be based on the resilience of still existing open woodlands. Long-term effects of a brief regeneration cycle offer a worthwhile situation to use rainfall in the most efficient way. Consequently, the 3–4 years following El Niño rainfalls might be of highest importance and be an enhanced necessity to support and control regeneration processes.

A rapidly expanding number of post-Niño fires after the extreme ENSO event in 1982/1983 are reported from the Galapagos Islands (Itow and Mueller-Dombois 1988). Hence, wildfires and droughts on the one hand as well as rainfalls and flooding on the other one must be considered El Niño driven disturbance or at least stress regimes in many parts of the tropical ecozone. This conclusion holds also true for much wetter Amazonian rainforests. While flooding effects are usually absorbed by adapted ecosystems such as igapó or várzea forests, regional extreme droughts in 1998, 2005, and 2010 caused large biomass burning and consecutive aerosol releases towards the eastern escarpment of the Andes. The climatic link of extraordinarily dry phases is coupled with unusually high SSTs in the tropical North Atlantic during July–December and most likely also with elevated SSTs during January–May, hence also during Super-Niño 97/98 (Coelho et al. 2012). The desiccation results from large-scale changes in the tropical atmospheric circulation forced by anomalous SST patterns affecting a monsoon-like precipitation regime in the Amazon. According to the aforementioned authors, the combination of El Niño conditions of high SSTs in the eastern and central Pacific and those in the tropical North Atlantic reinforce subsidence conditions in the Amazon, which are unfavorable to the occurrence of precipitation.

Although rainforest trees are prone to regulate their nutrient supply by an exuberant amount of small roots, especially the higher individuals dispose of additional deep-reaching roots in order to survive such phases of extraordinary desiccation stress. Apart from serving as ion pumps and as anchors, they also provide trees with water from phreatic resources.

Fig. 18 Annual versus EN 1997/1998 precipitation in northwestern Peru (*above*), three stages of vegetation development between October 1997 and April 2008 composed by three sketches and one aerial picture of the same plot 18 km wsw of Chulucanas (After Richter and Ise 2005, adjusted by recent material)

References

Allan R, Lindesay J, Parker D (1996) El Niño Southern Ocillation and climatic variability. CSIRO Publishing, Collingwood

Barry R, Chorley R (2003) Atmosphere, weather and climate. Routledge, London

Bendix A, Bendix J (2006) Heavy rainfall episodes in Ecuador during El Ni ño events and associated regional atmospheric circulation and SST patterns. Advances Geosci 6:43–49

Coelho CAS, Cavalcanti IAF, Costa SMS, Freitas SR, Ito ER, Luz G, Santos AF, Nobre CA, Marengo JA, Pezza AB (2012) Climate diagnostics of three major drought events in the Amazon and illustrations of their seasonal precipitation predictions. Meteorol Appl 19:237–255

Dando W (2005) Asia, Climates of Siberia, Central and East Asia. In: Oliver (deceased) J (ed) Earth sciences series. Encyclopedia of world climatology. Springer, Berlin/Heidelberg

Dash S (2005) Monsoons and monsoon climate. In: Oliver (deceased) J (ed) Earth sciences series. Encyclopedia of world climatology. Springer, Berlin/Heidelberg

Dekarski T, Praeg M, Wundram D, Richter M (2012) Tropical storms as triggers for intensified flooding and erosion processes in Southernmost Mexico. In: Cheval S (ed) InTech: natural disasters. InTech, Rijeke, Croatia, pp 87–120

Gnanadesikan A, Slater RD, Swathi PS, Vallis GK (2005) The energetics of ocean heat transport. J Climate 18:2604–2616

Hamann A (2004) Flowering and fruiting phenology of a Philippine submontane rain forest: climatic factors as proximate and ultimate causes. J Ecol 92:24–31

Heyer E (1998) Witterung und Klima: Eine Einführung in die Meteorologie und Klimatologie. In: Hupfer P, Kuttler W (eds) Witterung und Klima. Teubner, Stuttgart

http://math.ucr.edu/home/baez/soi-1876-1998.gif

http://www.bom.gov.au/climate/data/

http://www.jisao.washington.edu/data/cti/cti18502011.gif

http://en.wikipedia.org/wiki/File:Global_tropical_cyclone_tracks-edit2.jpg. Last assessed 3 May 2014

http://geology.com/articles/lightning-map.shtml. Last assessed 5 May 2014

http://www.atmos.washington.edu/%7Ehakim/301/hurr_cross.jpg. Last assessed 19 Feb 2014

http://www.fcst-office.com. Last assessed 5 May 2014

http://www.washingtonpost.com/blogs/capital-weather-gang/files/2013/11/1461780_624520054271903_1498249114_n.jpg. Last assessed 24 Apr 2014

Itow S, Mueller-Dombois D (1988) Population structure, stand-level dieback and recovery of *Scalesia pedunculata* forest in the Galápagos Islands. Ecol Res 3:333–339

Landscheidt T (2000) Solar forcing of El Niño and La Niña. ESA Special Publ 463:135–140

Lauer W (1993) Climatology. In: Pancel L (ed) Tropical forestry handbook, vol 1. Springer, Berlin/Heidelberg

McGregor GR, Nieuwolt S (1998) Tropical climatology. Wiley, Chichester

NCEP Reanalysis data: provided by the NOAA-CIRES ESRL/PSD Climate Diagnostics branch, Boulder, Colorado, USA, from their web site at http://www.cdc.noaa.gov/. Last assessed 15 Feb 2014

Nieuwolt S (1977) Tropical climatology. Wiley, London

Ramage C (1987) Monsoon climates. In: Fairbridge (deceased) R, Oliver (deceased) J (ed) Earth sciences series. Climatology. Springer, Berlin/Heidelberg

Richter M (1988) Gilbert – Kennwerte des stürmischsten Tages im karibischen "Jahrhundert-Hurrikan", 13.9.1988. Prax Geogr 18:57–59

Richter M (2001) Vegetationszonen der Erde. Klett-Perthes, Gotha

Richter M, Ise M (2005) Monitoring plant development after El Niño 1997/98 in northwestern Perú. Erdkunde 59:136–155

Ross MS, Meeder JF, Sah JP, Herndon A, Ruiz LP, Telesnicki G (1997) Windthrow in South Florida Pine Rocklands: pit-and-mound features and plant microhabitat associations following hurricane Andrew. www2.fiu.edu/%7Eprojects/windthrow/windthrow.html

Shultz JM, Russell J, Espinel Z (2005) Epidemiology of tropical cyclones: the dynamics of disaster, disease, and development. Epidemiol Rev 27:21–35

Vanselow K, Kolb M, Fickert T (2007) Destruction and regeneration of terrestrial, littoral and marine ecosystems on the Island of Guanaja/Honduras seven years after Hurricane Mitch. Erdkunde 61:358–371

WCRP (2013) World Climate Research Programme. http://www.wcrp-climate.org/WCRPevents2013.shtml. Last assessed 13 Feb 2014

Webster PJ (1987) The elementary monsoon. Wiley, New York